


Article

# Multi-Sensor GA-BP Algorithm Based Gearbox Fault Diagnosis

Yuan Fu , Yu Liu and Yan Yang \*

Department of Mechanical Engineering, Chongqing University of Technology, Chongqing 400054, China; fy@stu.cqut.edu.cn (Y.F.); liuyu@cqut.edu.cn (Y.L.)

\* Correspondence: yangyan@cqut.edu.cn

**Abstract:** To address the problem of the low recognition rate of time-frequency domain methods gearbox fault identification, a method featuring decision-level fusion of DS evidence theory and GA-BP algorithm was proposed in the present study. Firstly, the fault data of each state of the gearbox was classified, based on which the time-frequency domain features were extracted and 19 significant features have been selected. Secondly, the accuracy of the traditional BP algorithm was compared with that of the GA-BP algorithm. On this basis, it has been concluded that the GA-BP algorithm is highly accurate, and the local diagnostic results obtained by the GA-BP algorithm have been used as the basic probability. Finally, the DS evidence theory is currently used to fuse with the GA. In addition, the final fault identification of the gearbox can be achieved by using the DS evidence theory and the multi-sensor local diagnosis results obtained by the GA-BP algorithm for decision fusion. The results of the simulations and experiments showed that the method proposed has improved accuracy over a single algorithm for fault identification of gearboxes, respectively.

**Keywords:** gears; fault-diagnosis; GA-BP algorithm; DS fusion theory



**Citation:** Fu, Y.; Liu, Y.; Yang, Y. Multi-Sensor GA-BP Algorithm Based Gearbox Fault Diagnosis. *Appl. Sci.* **2022**, *12*, 3106. <https://doi.org/10.3390/app12063106>

Academic Editor: Alessandro Gasparetto

Received: 25 February 2022

Accepted: 16 March 2022

Published: 18 March 2022

**Publisher's Note:** MDPI stays neutral with regard to jurisdictional claims in published maps and institutional affiliations.



**Copyright:** © 2022 by the authors. Licensee MDPI, Basel, Switzerland. This article is an open access article distributed under the terms and conditions of the Creative Commons Attribution (CC BY) license (<https://creativecommons.org/licenses/by/4.0/>).

## 1. Introduction

Gearbox have been widely used in nuclear power gearboxes, wind turbines, cranes, and other fields. The gear faults will lead to low productivity and even serious injury and property damage, but it is difficult to detect due to the complex working environment. How to improve the ability of monitoring of gear health is important in industrial applications.

In terms of researches using traditional fault diagnosis methods, they tend to adopt data collected by a single sensor to perform time domain, frequency domain, and wavelet analysis on a physical quantity. A composite diagnosis method combined resonance-based sparse signal decomposition (RB-SSD) and maximum correlated kurtosis deconvolution (MCKD) for improvement of vibration signal fault recognition rate is proposed by He [1]. Based on the multi-channel fault identification method, Zhuang et al. [2] made use of the Empirical Mode Decomposition (EMD) method to convert the signal into a multi-channel one-dimensional signal, and then extracted and classified its features to realize the gearbox fault diagnosis and solve the fault. This has made up for the lack of fault identification features. Zhang et al. [3] monitored the health of the pick gear artificially and proposed to use the BP neural network algorithm to detect the faults of various characteristic signals collected. Due to the long iteration time and low accuracy of the traditional BP neural network, Zhang et al. [4] proposed Genetic Algorithm (GA) to perfect the traditional BP algorithm. Furthermore, the accuracy was improved after the improvement.

The detection status obtained by the classifier from a single sensor cannot comprehensively represent the health status. To this end, in recent years, Dempster-Shafer evidence theory (DS) multi-source information fusion technology has been widely used in the field of fault diagnosis [5–9]. Tang et al. [10] came up with a fusion method of random forest mixed classifiers, which realized the diagnosis of a single fault in a complex fault environment and significantly promoted the reliability of the diagnosis. In addition, Feng et al. [11] came up with a multi-source information fusion method that combines cloud theory and D-S

evidence theory for the ambiguity and uncertainty of multi-source fault signals. Furthermore, it has been verified by the fault diagnosis test of the rolling bearing of the Computer Numerical Control (CNC) machine tool. Zhou et al. [12] made use of the combination of D-S theory and support vector machine to diagnose the fault range and type of a structural beam. Yu et al. [13] thought out a decision-level fusion of the DS theory and the diagnostic results obtained by Support Vector Machines (SVM) to reduce the possibility of errors. Deep learning algorithms are also widely used in the field of fault diagnosis. Kadam et al. [14] proposed to combine deep learning algorithms and SVM algorithms for fault detection on the surface of 3D printed products, and the method enabled real-time monitoring in both offline and online states. Deep learning can detect squirrel cage induction motors (SCIMs) in early, Kumar et al. [15] proposed a novel fault detection technique for bearing faults and broken rotor bar detection in SCIM using the dilated convolutional neural network-based model. The propounded approach accomplished an average accuracy of more than 99.50%. In addition, Kamat et al. [16] proposed deep learning algorithm for estimating remaining bearing life, and it achieved an accuracy of over 90% in anomaly detection and Remaining Useful Life (RUL) prediction.

Huang et al. [17] proposed multi-feature fusion of the features obtained from the EMD method with some time-domain features as an input to the GA-BP algorithm to achieve fault diagnosis of bearings, which has a higher identification rate than using one feature vector. Li et al. [18] come up with an algorithmic fusion method that decompose the wavelet packet to acquire 8 energy ratios as features input to different classifiers, which can acquire their respective local diagnosis results. Finally, fused with DS evidence theory, and this method improved the rolling bearing diagnosis accuracy. Kumar et al. [19] proposed to base on collects real-time multi-sensor signals using vibration, current, and sound sensors. The convolutional neural network (CNN) algorithm is used for different fault signals to classify faults in 3D printed products with an accuracy of about 94%.

The multi-source information fusion technique can improve the accuracy, but when feature selection is carried out, only a certain part of time-domain features or frequency-domain features are considered, and the common time-frequency-domain features are not unified for feature selection. In addition, the GA-BP algorithm and DS fusion theory are fused at the data level and feature level to improve the fault diagnosis accuracy, but they are not fused at the decision level. Therefore, this study tries to select 19 common time-frequency domain feature indicators as features, and then use the DS theory and the local diagnosis results obtained by the GA-BP neural network algorithm for multi-sensor decision-level fusion, and apply the method to gear fault diagnosis as well. The fault diagnosis of the bearing inner ring of the bearing public data set of Case Western Reserve University has been used as a verification method. Moreover, the verification results have proven the effectiveness of the method. Then, a test bench for gear fault diagnosis was established to monitor the health of gear with varying pitting degrees. Both experiments and public datasets are able to verify that the proposed method is more accurate than traditional single-sensor fault detection.

## 2. Fundamental Theories

### 2.1. Multi-Sensor Information Fusion

Multiple linear acceleration sensors were used to obtain different sensitive signals at different points, and the time-frequency domain features were extracted. Then the extracted features were input into GA-BP algorithm to obtain local diagnosis results. Fusion of different local diagnosis results at the decision level. Finally, the fused diagnosis results were used for fault identification and classification. The decision-level fusion structure is shown in Figure 1.

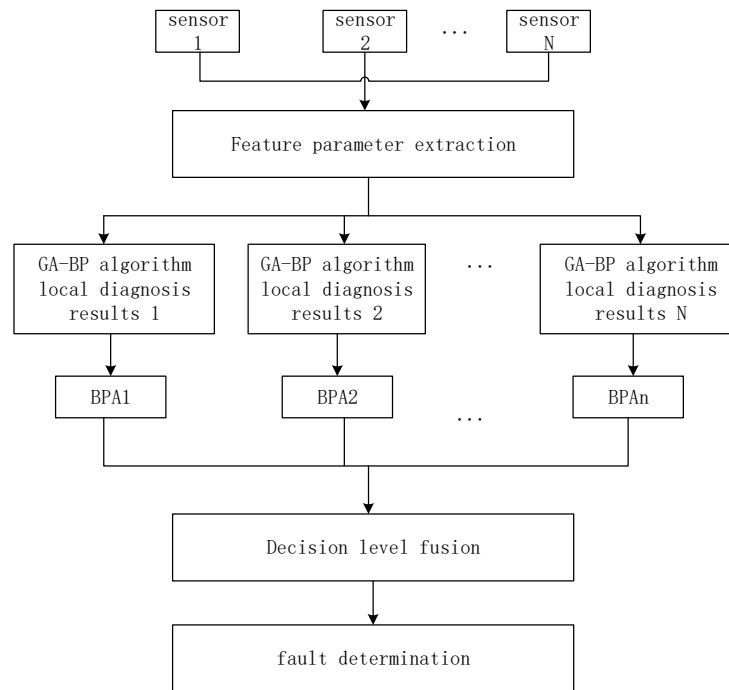


Figure 1. Multi-sensor decision-level fusion.

2.2. Time-Frequency Domain Feature Extraction

In terms of time-domain and frequency-domain features, common features: root mean square, root square amplitude, absolute mean, skewness, kurtosis, variance, maximum value, minimum value; barycentric frequency, mean square frequency, the frequency variance were mainly select.

In the time-frequency-domain feature analysis, the wavelet packet decomposition method can decompose the signal in a full frequency band and at multiple levels. It can make up for the shortcomings that wavelets cannot decompose low-frequency signals, and decompose high-frequency signals at a higher level, thus improving the decomposition rate of the entire signal frequency band. Therefore, the wavelet packet decomposition method is also widely used in the field of fault diagnosis. Wavelet packet signal decomposition diagram, as shown in Figure 2 [20]. Furthermore, the decomposed wavelet packet energy ratio was used as the time-frequency domain characteristic index. It is worth noting that the present study adopted three layers of wavelet packet decomposition. The function is db2.

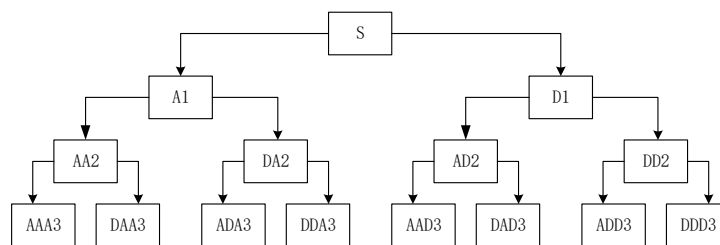


Figure 2. Wavelet Packet Signal Decomposition Diagram.

The wavelet packet is calculated as follows,

$$\begin{aligned}
 d_{i,j,2m} &= \sum_k h(k - 2i)d_{k,j+1,m} \\
 d_{i,j,2m+1} &= \sum_k g(k - 2i)d_{k,j+1,m}
 \end{aligned}
 \tag{1}$$

The wavelet packet reconstruction is calculated as follows,

$$d_{i,j+1,m} = \sum_k h(i - 2k)d_{k,j,2m} + \sum_k g(i - 2k)d_{i,j,2m+1} \tag{2}$$

where,  $d_{i,j,m}$  is the  $i$  wavelet packet coefficient of the  $m$  node of  $j$  the layer;  $h(k)$  and  $g(k)$  are the low-pass and high-pass filter coefficients in the filter.

The energy  $E_{i,j}$  on the different frequency bands is calculated as,

$$E_{i,j} = \sum_{k=1}^N |d_{i,j(k)}|^2, j = 0, 1, 2, \dots, 2^i - 1 \tag{3}$$

The wavelet packet energy ratio  $P_{i,j}$  is calculated as follows,

$$P_{i,j} = \frac{E_{i,j}}{\sum_{j=0}^{2^i-1} E_{i,j}} \tag{4}$$

### 2.3. BP Algorithm and GA-BP Algorithm

#### 2.3.1. BP Algorithm

The BP algorithm [21] is a multi-layer feedforward algorithm trained according to the error back-propagation algorithm. This algorithm enjoys strong self-learning ability, but poor generalization ability. It can easily fall into local extreme value state. The structure is shown in Figure 3 [18].

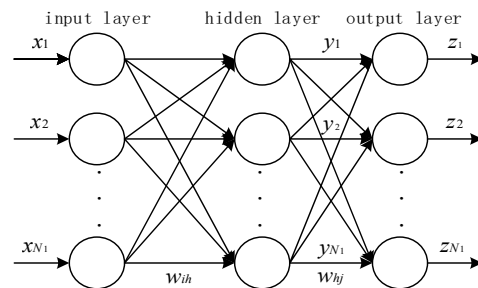


Figure 3. BP algorithm structure.

The method to determine the number of hidden layer nodes is calculated as follows [17],

$$m = \sqrt{(l + n)} + a \tag{5}$$

where  $l, m, n$  is input layer, hidden layer, and output layer, respectively. While  $a$  is a constant value ranging from 1 to 10.

#### 2.3.2. GA-BP Algorithm

The core of the genetic algorithm is mainly about the operation of selection, crossover, and mutation. The main purpose of using a genetic algorithm to optimize the BP algorithm is to obtain optimal connection weights and thresholds. To begin with, the neural network topology was determined and the initial weights and thresholds were generated, then, the genetic algorithm encoded the generated initial weights and thresholds to determine the fitness function. Finally, the selection, crossover, and variation operations were performed to bring the obtained optimal weights and thresholds into the network for training. The flow chart is shown in Figure 4.

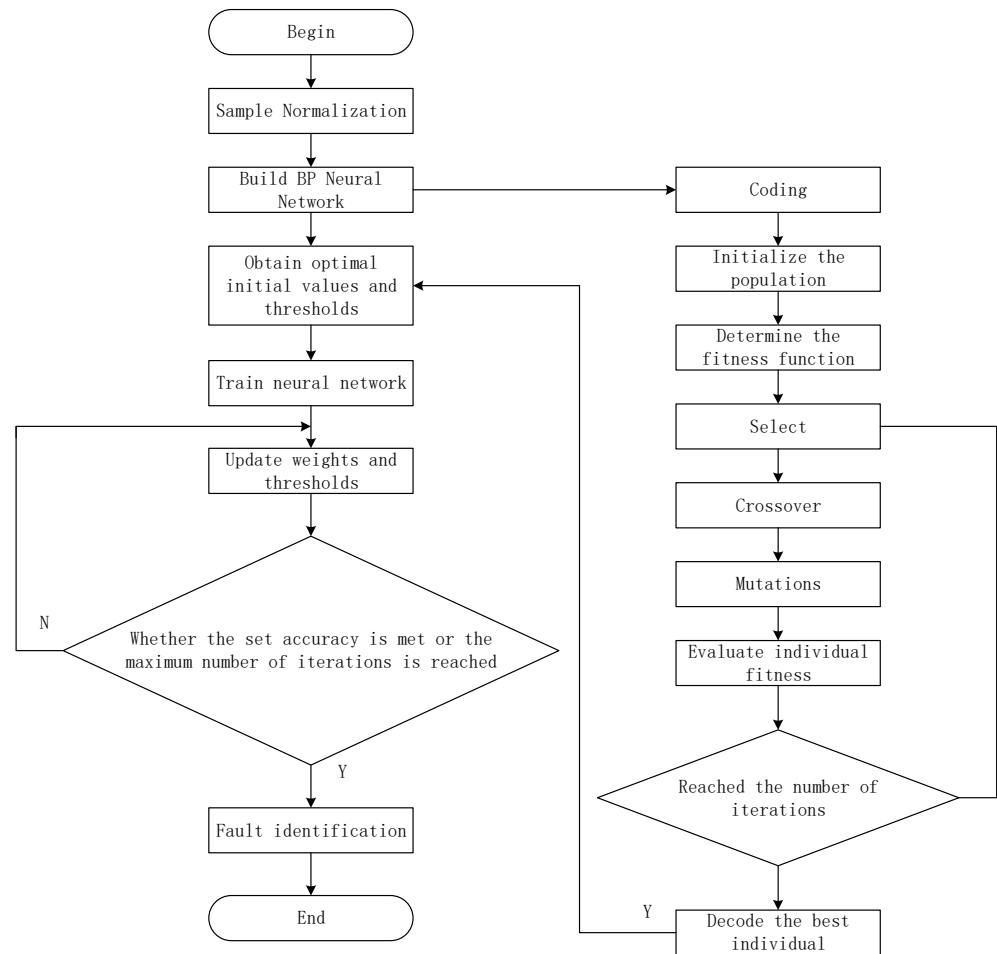


Figure 4. GA-BP algorithm fault identification block diagram.

2.4. DS Theory

DS evidence theory mainly includes identification framework, basic probability distribution function, trust function, and plausibility function. The identification framework of DS evidence theory is a finite and complete set composed of N pairs of mutually exclusive elements, usually represented by  $\Theta$ . The collection is shown below [22],

$$2^\Theta = \{\emptyset, \theta_1, \theta_2, \dots, \theta_N, \theta_1 \cup \theta_2, \dots, \theta_1 \cup \theta_2 \cup \theta_3, \dots, \Theta\} \tag{6}$$

DS evidence theory assigned a probability to each possibility in the identification framework, which is also known as the basic probability assignment (BPA). The basic probability distribution function is generally named a mass function. Furthermore, m is often used to represent this function. The power set  $2^\Theta$  of the recognition framework satisfied the following relation [23],

$$\begin{cases} 0 \leq m(A) \leq 1 \\ m(\emptyset) = 0 \\ \sum_{A \subseteq \Theta} m(A) = 1 \end{cases} \tag{7}$$

where, A is any subset in the identification frame, m(A) is the basic probability number of A.

In order to combine information from multiple independent sources, DS evidence theory provides DS fusion rules for achieving the fusion of multiple pieces of evidence. The combination rules are as follows [24],

$$\begin{cases} m(\emptyset) = 0 \\ m(A) = \frac{1}{1-k} \sum_{\cap A_i=A} \prod_{1 \leq i \leq N} m_i(A_i), A \neq \emptyset \\ k = \sum_{\cap A_i=\emptyset} \prod_{1 \leq i \leq N} m_i(A_i), k \neq 1 \end{cases} \quad (8)$$

where,  $k$  is the conflict coefficient.

### 3. Simulation Analysis

#### 3.1. Data Processing

The simulation data was from the Bearing Data Center of Case Western Reserve University in the United States. The sampling bearing model is 6205-2RS JEM SKF deep groove ball bearing, the motor speed is 1797 r/min, and the sampling frequency is 12 kHz. The four damage diameter states of the inner ring of the bearing: Normal, 0.007 inches, 0.014 inches, 0.021 inches, respectively, using (1, 2, 3, 4) to represent the fault state. The matrix form is [1 0 0 0], [0 1 0 0], [0 0 1 0], [0 0 0 1].

In this present study, the data of four-fault states of the inner ring of the bearing were selected, and the data of each state was divided into 29 groups with 4096 points in each group, a total of 116 groups of data. Then, a feature extraction was performed, and a total of 19 time-frequency domain feature indicators were selected. The time frequency processing results of these 19 feature indicators are shown in Table 1.

Table 1. Time-frequency characteristic parameters.

Sample	Time Domain Features			Frequency Domain Features			Time-Frequency Features		
	Root Mean Square	...	Kurtosis	Barycenter Frequency	...	P <sub>13</sub>	...	P <sub>83</sub>	
Normal	1	0.0823	...	0.0068	1161.104	...	45.6012	...	0.1492
	2	0.0846	...	0.0072	1123.906	...	44.6706	...	0.1578
	...	...	...	...	...	...	...	...	...
	29	0.0829	...	0.0069	1168.689	...	38.1235	...	0.1646
0.007"	1	0.2445	...	0.0598	2446.6	...	9.4725	...	1.0977
	2	0.2466	...	0.0608	2446.023	...	9.0168	...	1.1224
	...	...	...	...	...	...	...	...	...
	29	0.2470	...	0.0610	2500.594	...	8.4057	...	1.0324
0.014"	1	0.1252	...	0.0157	3126.209	...	16.9972	...	6.1315
	2	0.1286	...	0.0165	3136.342	...	17.2573	...	6.1819
	...	...	...	...	...	...	...	...	...
	29	0.1203	...	0.0145	3073.158	...	18.9016	...	5.3250
0.021"	1	0.2318	...	0.0537	2877.327	...	18.0769	...	1.5097
	2	0.2245	...	0.0504	2836.955	...	19.8080	...	1.7618
	...	...	...	...	...	...	...	...	...
	29	0.2259	...	0.0510	2846.9183	...	17.1866	...	1.9061

In each state, the front 20 sets of feature index data were selected for training. The remaining 9 sets of data were used as the test set. The training set is input into the BP algorithm and the GA-BP algorithm. At this point, the input layer is 19 layers and the output layer is 4 layers.

The value of  $a$  is dependent on the accuracy of output data and the Mean Squared Error (MSE) which MSE represents the fit of the model pair to the data. The accuracy and

the MSE at different values of  $a$  from 1 to 10 is calculated by Equation (5), respectively. The results are shown in Figure 5.

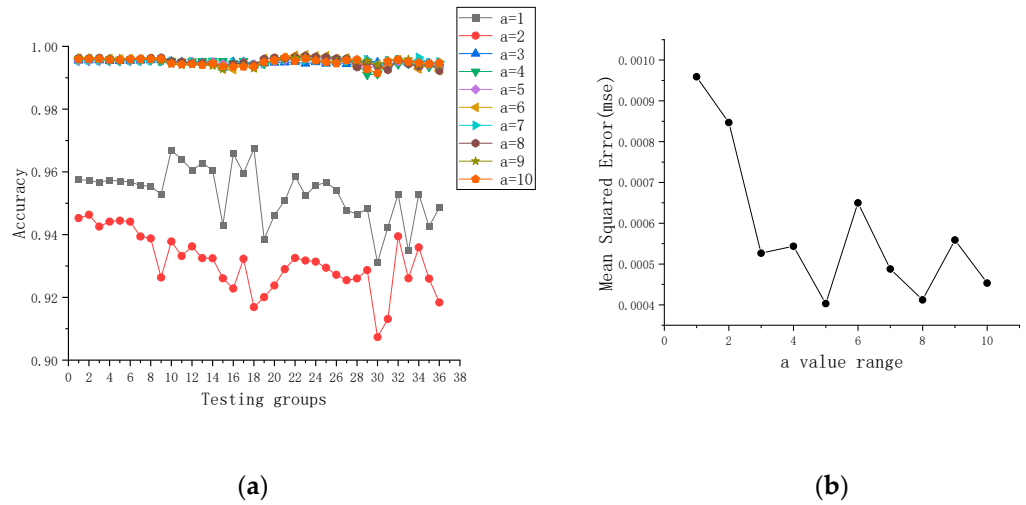


**Figure 5.** A value assessment. (a) Accuracy at different output values; (b) MSE at different model fit to data.

The accuracy rate is almost the same when the value of  $a$  is 3 to 10, and the fit of the model pair to the data is best when the value of  $a$  is 5. Then the optimal number of nodes in hidden layers can be concluded as 10.

Hence, the BP algorithm and the GA-BP structure are 19-10-4. The training results of four-fault states of bearings using the two algorithms are shown in Figures 6 and 7. According to figures, the BP algorithm needs 14 epochs (around 0.019 s), and the GA-BP algorithm only needs 7 epochs (around 0.009 s). It can be concluded that the operation speed of the GA-BP algorithm is faster. After the completion of this training, the remaining 9 groups of data of each state are used as the test data of the two algorithms for state recognition. The test data results are shown in Tables 2 and 3.

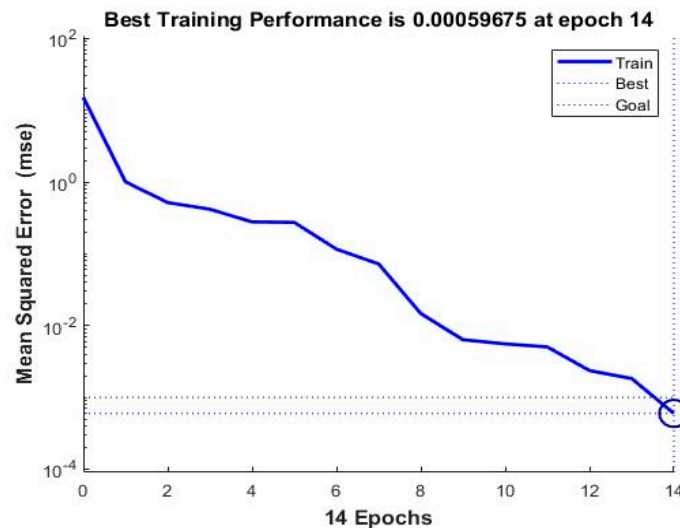


**Figure 6.** The number of iterations of the BP algorithm.

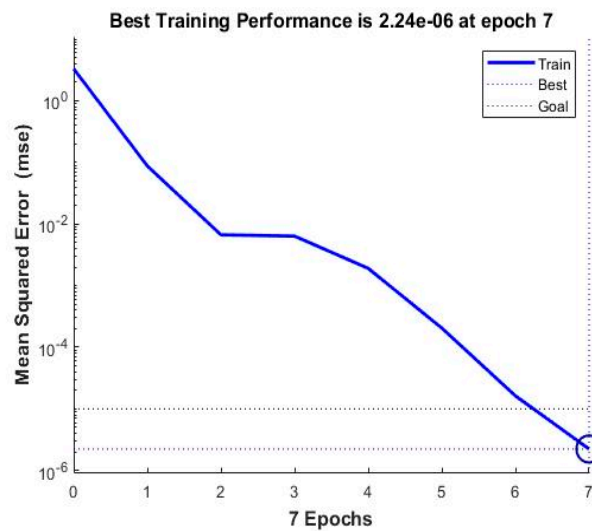


Figure 7. The number of iterations of the GA-BP algorithm.

Table 2. BP algorithm test data.

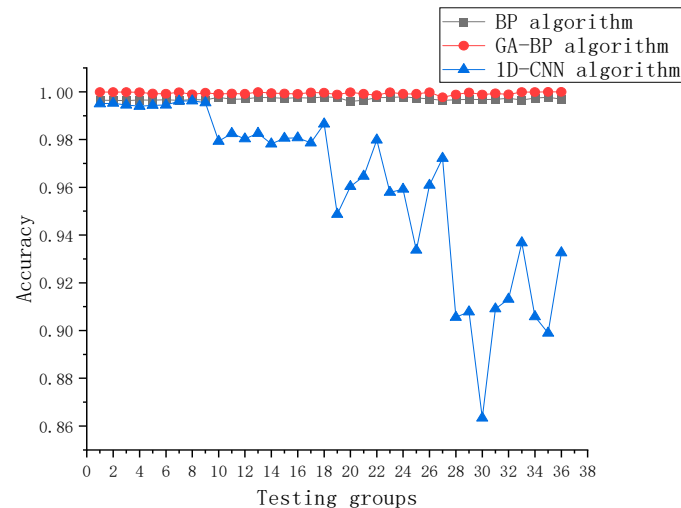
Sample	Test Data				Fault
1	0.99770	0.00045	0.00069	0.00041	1
2	0.99773	0.00044	0.00075	0.00036	1
...	...	...	...	...	...
9	0.99746	0.00245	0.00061	-0.0015	1
1	0.00008	0.99924	-0.00009	0.00185	2
2	-0.00011	0.99989	-0.00009	0.00231	2
...	...	...	...	...	...
9	-0.00004	0.99828	0.00022	0.00306	2
1	0.00088	-0.0006	0.99893	0.00153	3
2	0.00082	-0.0010	0.99942	0.00151	3
...	...	...	...	...	...
9	0.00056	-0.0003	0.99911	0.00126	3
1	0.00262	-0.0022	0.00028	1.00032	4
2	0.00150	0.00057	0.00068	0.99861	4
...	...	...	...	...	...
9	0.00300	-0.00165	-0.00007	0.99899	4

Table 3. GA-BP algorithm test data.

Sample	Test Data				Fault
1	1.00060	0.00851	0.00863	0.00106	1
2	1.00114	-0.00561	0.00484	0.00142	1
...	...	...	...	...	...
9	1.00023	0.00005	-0.00362	0.00738	1
1	0.00865	0.99963	0.00050	0.00063	2
2	0.00613	1.00053	0.00490	0.00860	2
...	...	...	...	...	...
9	0.00901	1.00047	0.00635	0.00399	2
1	0.00575	0.00282	1.00095	0.00134	3
2	0.00845	0.00539	1.00051	0.00031	3
...	...	...	...	...	...
9	0.00661	-0.00853	1.00067	0.00025	3
1	0.00730	0.00874	0.00842	1.00216	4
2	0.00891	0.00270	0.00559	1.00057	4
...	...	...	...	...	...
9	0.00121	-0.00082	0.00331	1.00024	4



The GA-BP algorithm is compared with the BP algorithm by means of the performance metrics of mean square error, number of iterations, time required, speed of convergence, and accuracy. In addition, one-dimensional convolutional neural network (1D-CNN) in machine learning was used to compare the accuracy of the BP algorithm and the GA-BP algorithm in simulation and experiment. The accuracy comparison of these algorithms are shown in below Figure 8.



**Figure 8.** Accuracy of the three algorithms.

As shown in Figure 8, three algorithms are relatively volatile. However, the GA-BP algorithm is 2.3% more accurate than the traditional BP algorithm and GA-BP algorithm is 3.99% more accurate than the traditional 1D-CNN algorithm.

### 3.2. DS Evidence Synthesis and Decision-Level Fusion

A single sensor in traditional fault diagnosis methods can lead to a lack of comprehensiveness of data. Hence, multi-sensor testing of gearboxes is needed. In order to perform fault diagnosis on fault data collected from multiple sensors, the decision-level fusion of the multi-sensor local diagnostic results obtained by the GA-BP algorithm using a DS-theoretical approach would be able to capture the multidimensionality of the data and improve the diagnostic accuracy.

In addition, the GA-BP algorithm allows for the fault diagnosis of gears from the fault data collected by each sensor. The DS theory was used to fuse the local diagnostic results of each sensor at the decision level. The identification framework needs to be established first based on DS evidence theory. Furthermore, since there are four fault states, the identification framework is  $\Theta = \{A, B, C, D\}$ , corresponding to bearing fault states: Normal, 0.007 inches, 0.014 inches, and 0.021 inches, respectively. An objective body of evidence needs to be identified, with the body of evidence  $E = \{E1, E2\}$  in order to achieve effective fusion of diagnostic results. The E1 represents the bearing fan-end sensor and E2 represents the bearing base-end sensor. The fusion rule of Equation (8) was then used to fuse the local diagnostic results of the two sensors to obtain the fused bearing fault diagnosis rate. The fault diagnosis results before and after fusion are shown in Figure 9.

According to Figure 9, it can be concluded that the accuracy of the two bodies of evidence is 99.92% and 99.93% before the fusion. The accuracy after fusion was 99.99%. The accuracy after adopting fusion theory was significantly higher than that before fusion and more stable, compensating for the low accuracy of the traditional single fault diagnosis method to a large extent.

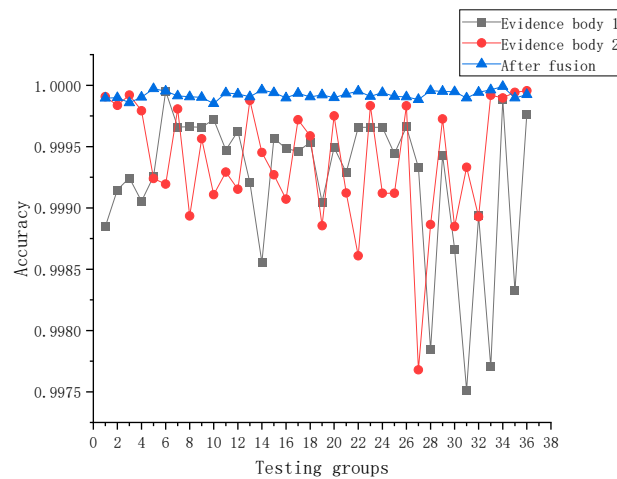


Figure 9. Diagnostic results before and after fusion of evidence.

### 4. Experiments

#### 4.1. Experimental Data Acquisition

There are 19 input parameters, which include 8 time-domain parameters, 3 frequency-domain parameters, and 8 energy ratios of the Wavelet Packet of 3-layer decomposition. Time-domain parameters include root mean square, root square amplitude, absolute mean, skewness, kurtosis, variance, maximum value, and minimum value. The frequency-domain features include barycentric frequency, mean square frequency, and the frequency variance. In addition, time-frequency indicators include  $P_{13}$ ,  $P_{23}$ ,  $P_{33}$ ,  $P_{43}$ ,  $P_{53}$ ,  $P_{63}$ ,  $P_{73}$ , and  $P_{83}$ . As shown in Table 1, due to limited space, not all are listed.

According to the working data of the nuclear gearbox gears provided by the cooperative enterprise, the gear speed was set to 480 r/min, 650 r/min, 750 r/min and 800 r/min. As shown in Table 4 for the experimental conditions.

Table 4. Experimental gear example conditions.

Load (N.m)	Number of Experiments	Sampling Time (Seconds)	Sampling Frequency (KHz)	Rotating Speed (r/min)
20	20	1	5	480
				650
				750
				800
			10	480
				650
				750
				800

Due to the presence of multiples in the frequency of engagement in the experiment. According to Nyquist’s principle, the sampling frequency is 10 KHz to ensure that no distortion occurs in the signal. When carrying out the effect of speed on the results, the most significant change in signal was found at 800 r/min. Therefore the experimental conditions were chosen as, the sampling frequency is 10 KHz, the speed is 800 r/min and the load is 20 N.m.

As shown in Table 5 for the gear condition,

**Table 5.** Experimental gear example.

Condition	Pitting Area (mm <sup>2</sup> )	Pitting Location
Normal	0	
Single tooth single pitting	0.785	Near the node line
Single tooth double pitting	1.57	
Single tooth three pitting	2.34	

In order to verify the effectiveness of the proposed method in practical production, the experimental data collected on the gearbox test bench have been used for gear fault diagnosis. To this end, the test rig was designed first, the linear acceleration sensor mounting position arrangement selected, the gear selection and other equipment configuration, and the test bench structure diagram, shown in Figure 10. For the next, the gear fault detection test bench was established, as shown in Figure 11. The test bench consists of a gearbox (including a large gear with 36 teeth and a small gear with 25 teeth), drive motors, and so on. Three acceleration sensors were mounted in the gearbox housing near the vibration source. Three acceleration sensors were mounted in the gearbox housing near the vibration source.

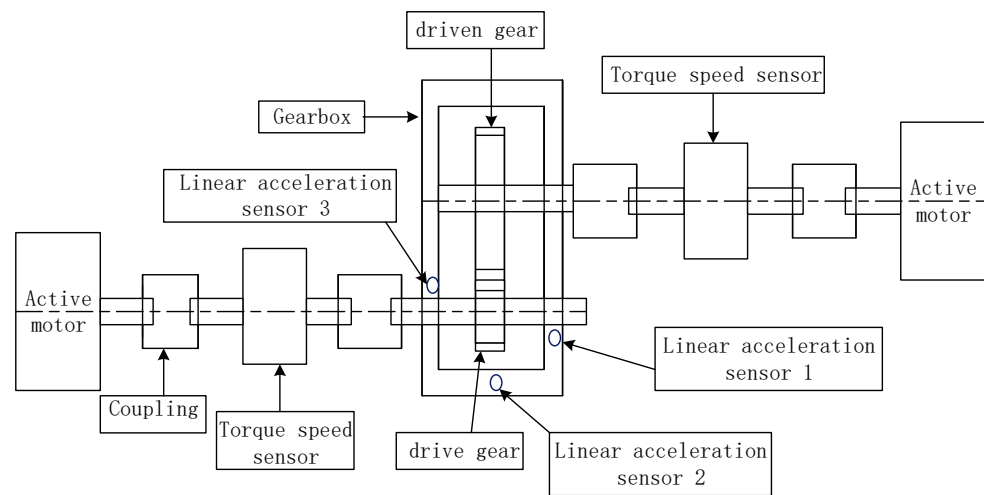


**Figure 10.** Structural design of the gear test bench.

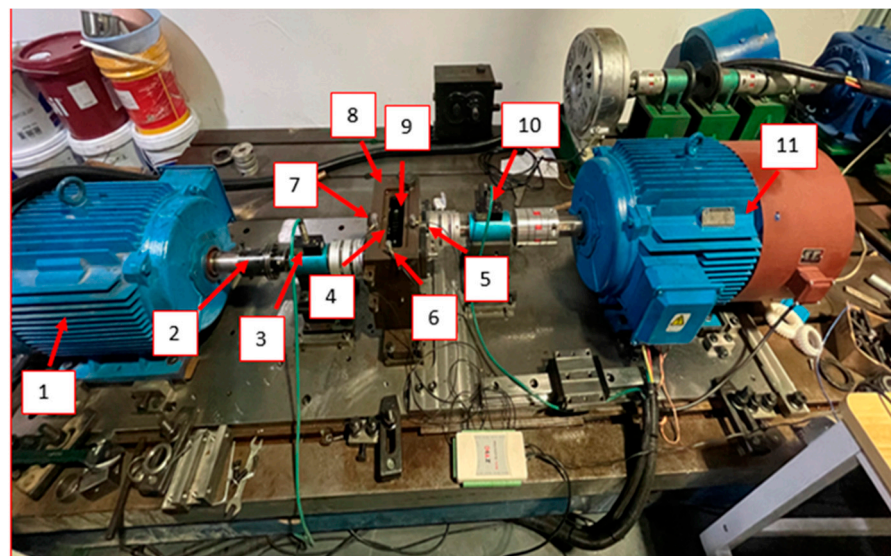


**Figure 11.** Gear test bench set up. 1,11-Active motor, 2-Coupling, 3,10-Torque speed sensor, 4-drive gear, 5,6,7-Linear acceleration sensor, 8-Gearbox, 9-driven gear.

The experiment focuses on the health monitoring of an active gear with four states: normal, single pitting, double pitting, and triple pitting, respectively, using (1, 2, 3, 4) to represent the fault state. The matrix form is  $[1\ 0\ 0\ 0]$ ,  $[0\ 1\ 0\ 0]$ ,  $[0\ 0\ 1\ 0]$ ,  $[0\ 0\ 0\ 1]$ . The degree of the condition is shown in Figure 12. The collected experimental data for each state is divided into 48 groups, each group of data consists of 4096 points, with a total of 192 groups of experimental data vibration signal for each state. Please refer to Figure 13.

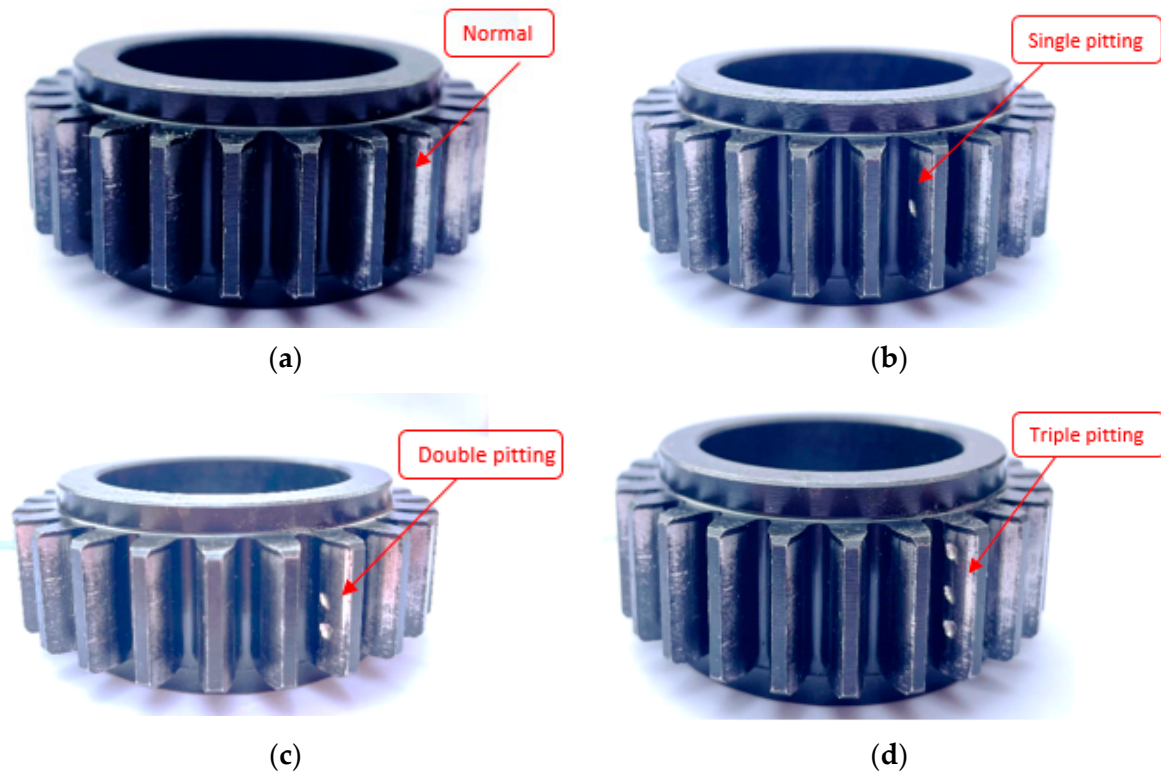


**Figure 12.** Gears with different degrees of pitting. (a) Normal condition, (b) single pitting condition, (c) double pitting condition, (d) triple pitting condition.

By selecting the frequency domain features from the grouped experimental data, 19 common time-frequency domain features can be extracted. Each state can thus constitute of points, simplifying the original data set and largely improving the speed of gear fault monitoring operations.

In each state, the front 34 sets of data are selected for training and the remaining 14 sets are used as the test set. The training set is fed into the BP algorithm and the GA-BP algorithm, at this point, the input layer is 34 layers, the output layer is 4 layers, and the hidden layer is obtained according to Equation (5), where 10 layers were selected. Therefore, the structure of the BP algorithm and the GA-BP algorithm are 34-10-4. The data from the training set is first fed into the diagnostic model, and then the remaining 14 sets are fed into the diagnostic model as a test set for fault testing. The test results of the two algorithms are shown in Tables 6 and 7. The speed of the two algorithms is shown in Figures 14 and 15, and the accuracy is shown in Figure 16.

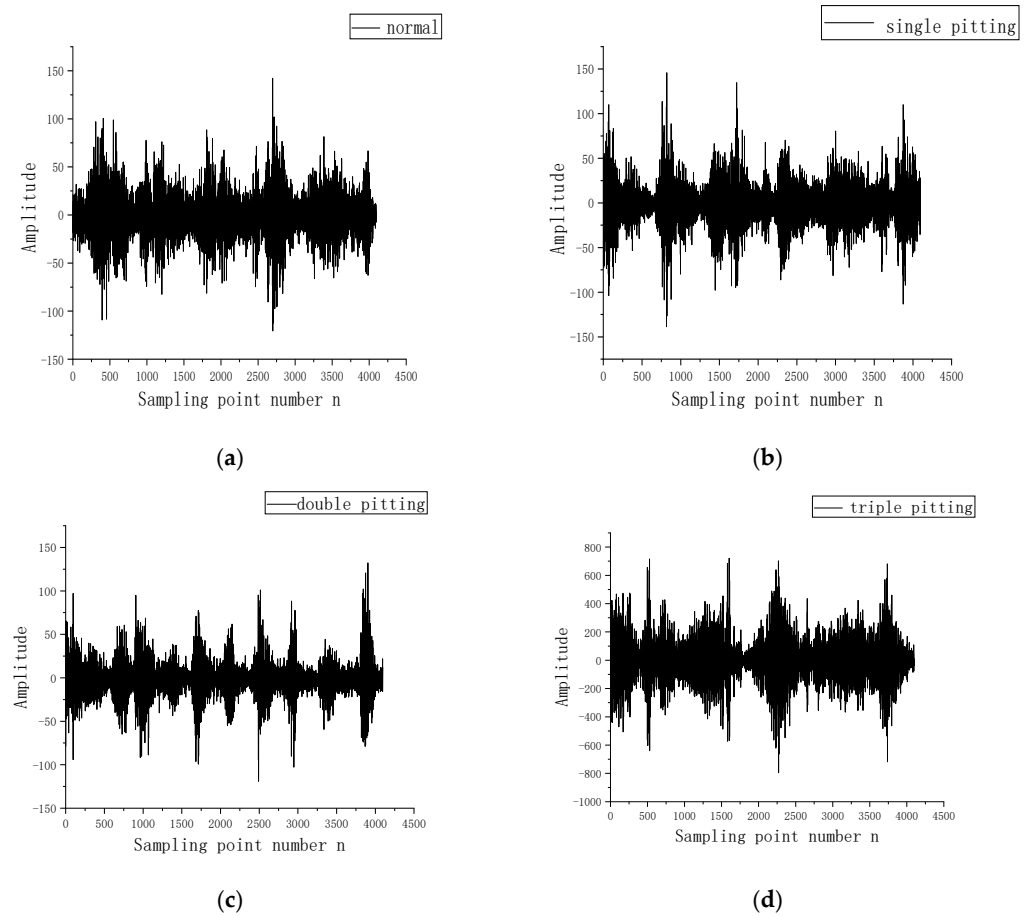


**Figure 13.** Vibration signals for 4 types of gear health monitoring. (a) Normal condition, (b) single pitting condition, (c) double pitting condition, (d) triple pitting condition.

**Table 6.** BP algorithm experimental test data.

Sample	Test Data				Fault
1	1.000506	0.033438	−0.03357	−0.00037	1
2	1.009513	2.120288	−2.13004	0.000242	1
...	...	...	...	...	...
14	0.999489	0.016411	−0.01581	$−8.5 \times 10^{-5}$	1
1	−0.00104	1.303728	−0.30177	−0.00092	2
2	0.00067	0.856819	0.142685	−0.00017	2
...	...	...	...	...	...
14	0.011091	1.862498	−0.87288	−0.0007	2
1	0.000317	0.652486	0.347745	−0.00055	3
2	−0.00145	1.01321	−0.01084	−0.00092	3
...	...	...	...	...	...
14	−0.00106	0.30225	0.700755	−0.00194	3
1	$7.07 \times 10^{-5}$	−0.00017	0.000117	0.999984	4
2	$7.16 \times 10^{-5}$	−0.00048	0.000427	0.999984	4
...	...	...	...	...	...
14	$6.84 \times 10^{-5}$	−0.00027	0.000219	0.999984	4

**Table 7.** GA-BP algorithm experimental test data.

Sample	Test Data				Fault
1	1.002133	0.001423	0.004012	0.002554	1
2	1.000103	0.005562	0.007136	0.003179	1
...	...	...	...	...	...
14	1.000276	0.006608	0.008686	0.004462	1
1	0.0055	1.00047	0.008853	0.009767	2
2	0.005802	1.000651	0.006563	0.007881	2
...	...	...	...	...	...
14	0.007025	1.000013	0.002331	0.009472	2
1	0.009201	0.009637	1.002577	0.009345	3
2	0.007863	0.007472	1.000319	0.009347	3
...	...	...	...	...	...
14	0.00661	−0.00853	1.00067	0.00025	3
1	0.001398	0.006349	0.007977	1.000525	4
2	0.000851	0.007368	0.006932	1.001214	4
...	...	...	...	...	...
14	0.008507	0.005294	0.001008	1.000231	4

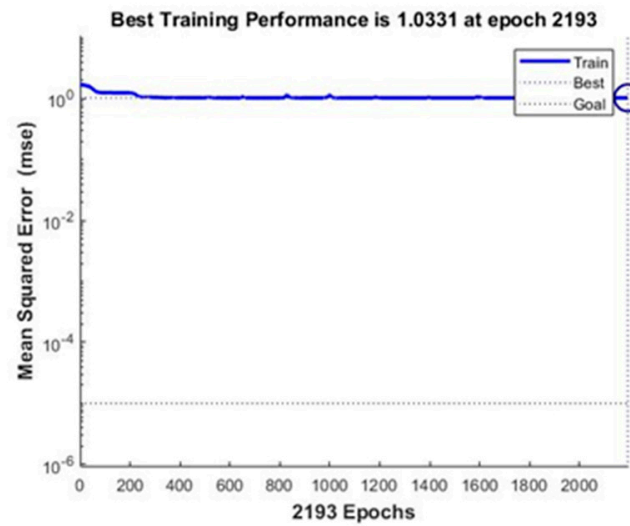


**Figure 14.** The number of iterations of the BP algorithm.

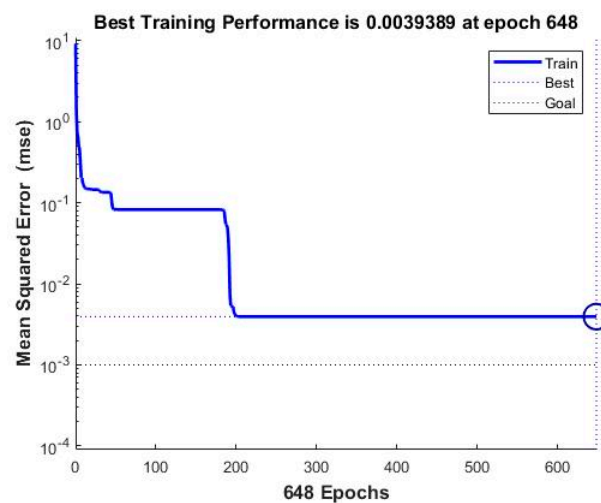


**Figure 15.** The number of iterations of the GA-BP algorithm.

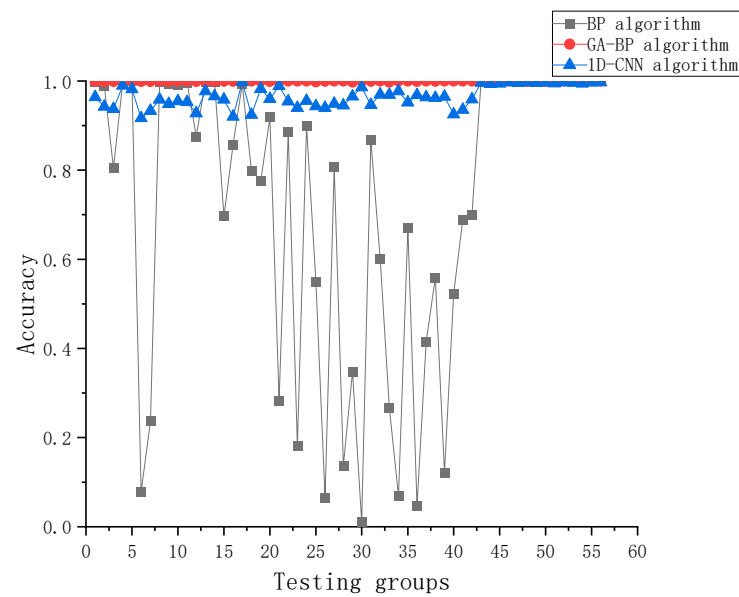


**Figure 16.** Accuracy of the three algorithms.

As shown in Figures 14 and 15, the number of iterations tested using the BP algorithm was 2193 epochs (around 3 s). While the number of iterations using the genetic algorithm was 648 epochs (around 0.886 s), which is 2.38 times faster convergence during testing. From the Figure 16, we can also see that the GA-BP algorithm has a higher accuracy than the BP algorithm.

According to Figure 16, among the three algorithms, the BP algorithm is the most volatile and the GABP algorithm is the most stable. The accuracy of the GA-BP algorithm is 27.26% higher than that of the traditional BP neural network algorithm, and it is also 3.48% higher than that of the traditional 1D-CNN algorithm.

The advantage of 1D-CNN is that it can effectively learn the corresponding features from a large number of samples, avoiding the complicated feature extraction process, with less manual involvement and high accuracy, which is very popular in the field of fault diagnosis. Only in this experiment, as the authors did not study 1D-CNN in depth, only a simple comparison with other algorithms was performed. If it is deeply optimized, the accuracy rate will definitely be improved substantially. However, the method of GA-BP proposed in this paper also can be accepted.

#### 4.2. DS Evidence Theory Fusion

Given that this experiment was carried out for four-fault states against fault diagnosis, the identification framework obtained was as follows.

A, B, C, and D correspond to the gear fault status of normal, single tooth single pitting, single tooth double pitting, and single tooth triple pitting, respectively. The three sensors {E1, E2, E3} were selected for data collection from the gearbox. DS evidence theory is mainly the fusion of multiple sensors. Thus, it can constitute four groups of evidence bodies E, respectively:  $E = \{E1, E2\}$ ,  $E = \{E1, E3\}$ ,  $E = \{E2, E3\}$ ,  $E = \{E1, E2, E3\}$ . After evidence bodies were determined, the fusion rules of Equation (8) were used to fuse the local diagnostic results of two sensors to obtain the fused bearing fault diagnosis rate, the fault diagnosis accuracy of each evidence body before and after fusion. Please refer to Figure 17.

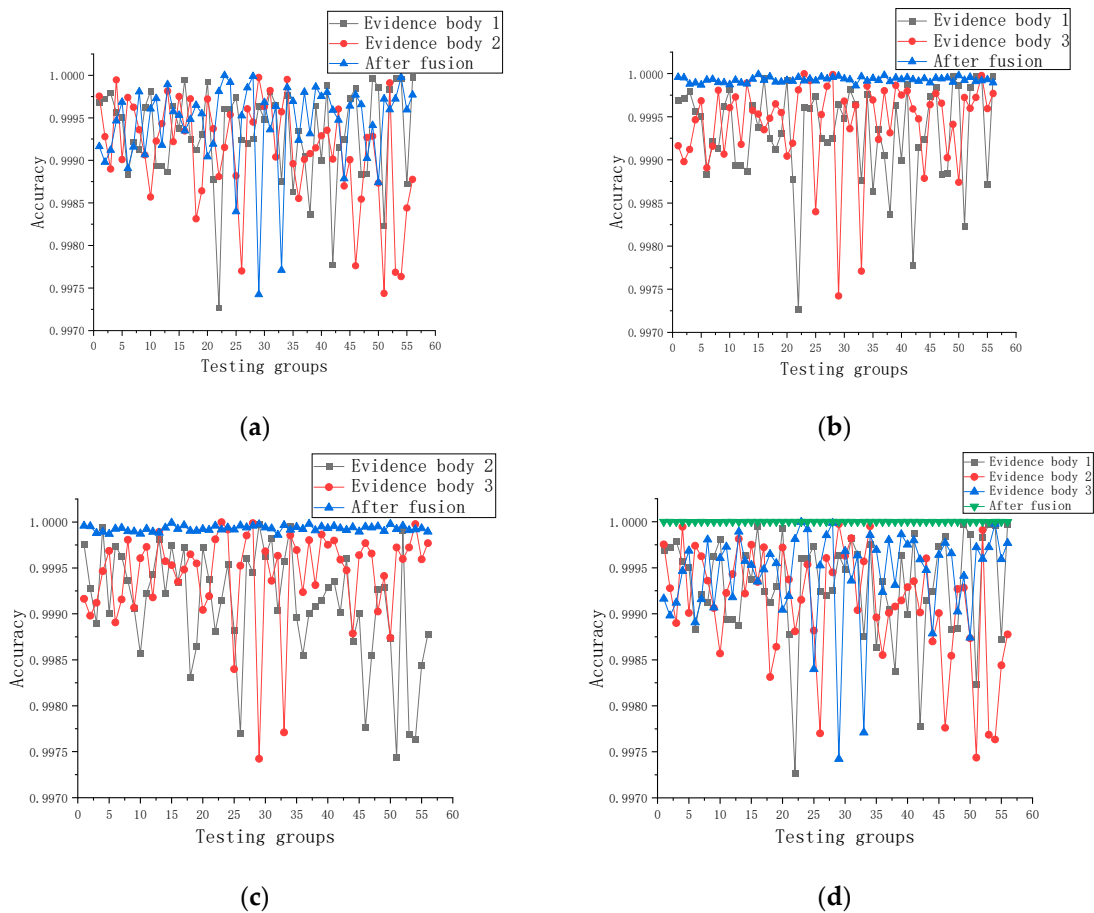


**Figure 17.** Diagnostic accuracy before and after gear fusion. (a) Fusion of evidence body 1 and evidence body 2, (b) fusion of evidence body 1 and evidence body 3, (c) fusion of evidence body 2 and evidence body 3, (d) 3 bodies of evidence fused.

According to Figure 16, before fusion, the accuracy of the three evidence bodies were 99.93%, 99.91% and 99.94%, respectively; when evidence body 1 was fused with evidence body 2, the accuracy after fusion increased by 0.12% and 0.33%, respectively; when evidence body 1 was fused with evidence body 3, the accuracy after fusion rose by 0.61%, and 0.50%, respectively; when evidence body 2 was fused with evidence body 3, the accuracies after fusion elevated by 0.82% and 0.50%, respectively; when the three evidence bodies were fused simultaneously, the accuracy after fusion was 99.99%, then the accuracies went up by 0.68%, 0.89% and 0.56%, respectively. The accuracy after using fusion theory was significantly higher than before fusion and was more stable than usual, compensating for the low accuracy of traditional single fault diagnosis methods to a large extent. However, when two sensors for fusion were used, the accuracy after fusion was not as good as the accuracy of all three sensors fused at the same time. Hence, the multidimensional information of the gears needs to be detected carefully, which can significantly improve the diagnosis accuracy of gears.

#### 4.3. Analysis of Experimental Results

The experimental results showed that the fault diagnosis of a single sensor using the GA-BP algorithm was 27.26% more accurate than using the BP algorithm. Nonetheless, given that the cause of the fault was not caused by a single factor, multi-dimensional extraction of the fault data is required to ensure the comprehensiveness of the data. Fusing the local diagnostic results from three sensors of the GA-BP algorithm subject to DS theory simultaneously, the accuracy of the fusion improved by 0.68%, 0.89%, and 0.56%, respectively, compared to the single sensor fault diagnosis rate using GA-BP and was



more accurate than the two-by-two sensor fusion. It implies that the gear data needs to be extracted for comprehensiveness in detecting health status. Although the accuracy rate before fusion has reached more than 99.90%, the accuracy rate will be improved after the new method is adopted, which shows that the proposed method is meaningful for the accuracy of gear fault diagnosis.

## 5. Conclusions

This present study addressed the lack of comprehensiveness and accuracy in detecting gear fault health status by means of traditional fault-diagnosis, and proposed a gear fault diagnosis method based on DS evidence theory for multi-sensor decision-level fusion of the local diagnosis results of GA-BP neural networks.

The proposed method has been proven to be a good remedy for the singularity of traditional diagnostic methods and improving the accuracy of the results. Firstly, both simulation and experiment can verify the high accuracy of the improved BP algorithm to address the problem of single sensor fault diagnosis accuracy, by comparing the fault detection accuracy of the BP algorithm before and after improvement using GA-BP, the diagnosis result using GA-BP neural network algorithm was chosen as the basic probability; secondly, as multiple sensors installed in the gearbox housing can monitor the health condition of the gear at the same time improving the detection accuracy, the local diagnosis result of GA-BP algorithm is fused at decision level using DS evidence theory.

**Author Contributions:** Y.Y. conceived this research; Y.F. and Y.L. deduced the calculation; Y.F. and Y.L. wrote the original draft preparation; editing and review on this article was completed by Y.Y.; Y.Y. is responsible for overseeing the progress and visualization of the article. All authors have read and agreed to the published version of the manuscript.

**Funding:** This research was funded by the National Key R&D Program of China (2020YFB2010103), the National Natural Science Foundation of China (No.51875068, No.52075062), the Graduate Student Innovation Program of Chongqing University of Technology (No. CYS21465).

**Institutional Review Board Statement:** Not applicable.

**Informed Consent Statement:** Not applicable.

**Data Availability Statement:** Not applicable.

**Acknowledgments:** The authors want to gratefully acknowledge the National Key R&D Program of China (2020YFB2010103), the National Natural Science Foundation of China (51875068, 52075062), and the Graduate Student Innovation Program of Chongqing University of Technology (CYS21465) for their support. Finally, the authors want to thank the editors and reviewers for their valuable comments and constructive suggestions.

**Conflicts of Interest:** The authors declare no conflict of interest. In addition, the funders had no role in the design of the study; in the collection, analyses, or interpretation of data; in the writing of the manuscript, or in the decision to publish the results.

## References

1. He, Q.; Guo, Y.; Wang, X.; Reng, Z.; Li, J. Gearbox fault diagnosis based on signal resonance sparse decomposition and maximum correlation cliff deconvolution. *China Mech. Eng.* **2017**, *28*, 7.
2. Ye, Z.; Yu, J. Gearbox vibration signal feature extraction based on multi-channel weighted convolutional neural network. *J. Mech. Eng.* **2021**, *57*, 110–120.
3. Qiang, Z.; Liu, Z.; Wang, Z.; Zhang, H. Research on multi-feature signal fusion recognition of wear degree of cut-off teeth. *J. Eng. Des.* **2018**, *25*, 10.
4. Zhang, F.; Zhang, X.; Chen, L.; Sun, L.; Zhan, W. Optimized neural network for binocular camera calibration using improved genetic algorithm. *China Mech. Eng.* **2021**, *32*, 1423–1431.
5. Chen, C.; Nie, D.; Feng, Z.; Zhang, X.; Zhao, K.; Shi, Y. Transformer fault diagnosis techniques based on probabilistic output support vector machines and evidence theory. *Transformer* **2018**, *55*, 58–61.
6. Liu, J.; Zhou, M.; Hou, C. Fault diagnosis of mechanical characteristics of circuit breakers based on quantum genetic neural network and D-S evidence theory. *High Volt. Electr.* **2018**, *54*, 7.

7. Li, J. Intelligent diagnosis of wind turbine faults based on evidence theory and support vector machines. *J. Jilin Univ. Sci. Ed.* **2016**, *54*, 4.
8. Moosavian, A.; Khazaee, M.; Najafi, G.; Kettner, M.; Mamat, R. Spark plug fault recognition based on sensor fusion and classifier combination using Dempster–Shafer evidence theory. *Appl. Acoust.* **2015**, *93*, 120–129. [[CrossRef](#)]
9. Ji, X.; Ren, Y.; Tang, H.; Shi, C.; Xiang, J. An intelligent fault diagnosis approach based on Dempster–Shafer theory for hydraulic valves. *Measurement* **2020**, *165*, 108129. [[CrossRef](#)]
10. Tang, X.; Gu, X.; Rao, L.; Lu, J. A single fault detection method of gearbox based on random forest hybrid classifier and improved Dempster–Shafer information fusion. *Comput. Electr. Eng.* **2021**, 107101. [[CrossRef](#)]
11. Feng, C.; Tan, J.; Sun, X. Research and experiment on multi-source information fusion method based on cloud model and evidence theory. *Manuf. Technol. Mach. Tools* **2015**, *11*, 87–93.
12. Zhou, Q.; Zhou, H.; Zhou, Q.; Yang, F.; Luo, L.; Li, T. Structural damage detection based on posteriori probability support vector machine and Dempster–Shafer evidence theory. *Appl. Soft. Comput.* **2015**, 368–374. [[CrossRef](#)]
13. Yu, K.; Tan, J.; Li, S. A brief research on rolling bearing fault diagnosis based on multi-sensor information fusion. *Instrum. Technol. Sens.* **2016**, *1*, 97–102, 107.
14. Kadam, V.; Kumar, S.; Bongale, A.; Wazarkar, S.; Kamat, P.; Patil, S. Enhancing Surface Fault Detection Using Machine Learning for 3D Printed Products. *Appl. Syst. Innov.* **2021**, *4*, 34. [[CrossRef](#)]
15. Kumar, P.; Hati, S. Dilated convolutional neural network based model for bearing faults and broken rotor bar detection in squirrel cage induction motors. *Expert Syst. Appl.* **2022**, *191*, 116290. [[CrossRef](#)]
16. Kamat, P.; Sugandhi, R.; Kumar, S. Deep learning-based anomaly-onset aware remaining useful life estimation of bearings. *PeerJ Comput. Sci.* **2021**, *7*, e795. [[CrossRef](#)] [[PubMed](#)]
17. Huang, W.; Wang, L.; Liu, J.; Chen, B. Fault identification of rolling bearings based on multi-feature fusion and GA-BP model. *Mach. Tools Hydraul.* **2021**, *49*, 5.
18. Li, R.; Zhang, G.; Wang, H.; Wang, X.; Song, Y.; Qi, L.; Reng, Y. Multi-sensor bearing fault diagnosis based on GA-BP neural network. *Chem. Autom. Instrum.* **2017**, *44*, 6.
19. Kumar, S.; Kolekar, T.; Patil, S.; Bongale, A.; Kotecha, K.; Zaguia, A.; Prakash, C. A Low-Cost Multi-Sensor Data Acquisition System for Fault Detection in Fused Deposition Modelling. *Sensors* **2022**, *22*, 517. [[CrossRef](#)] [[PubMed](#)]
20. Liu, X.; Han, J.; Xu, H.; Xiao, X.; Wen, Z.; Liang, S. An indirect method for rail corrugation measurement based on numerical models and wavelet packet decomposition. *Measurement* **2022**, *191*, 110726. [[CrossRef](#)]
21. Yuan, P.; Mao, J.; Xiang, F.; Liu, L.; Zhang, M. Improved genetic optimization based BP neural network for grid fault diagnosis. *J. Power Syst. Autom.* **2017**, *29*, 5.
22. Xiao, F. Multi-sensor data fusion based on the belief divergence measure of evidences and the belief entropy. *Inf. Fusion* **2019**, *46*, 23–32. [[CrossRef](#)]
23. Che, X.; Mi, J.; Chen, D. Information fusion and numerical characterization of a multi-source information system. *Knowl. Based Syst.* **2018**, *145*, 121–133. [[CrossRef](#)]
24. Gu, J.; Xie, D.; Gu, C.; Miao, J.; Zhang, Y. Location of low-frequency oscillation sources using improved D-S evidence theory. *Int. J. Electr. Power Energy Syst.* **2021**, *125*, 106444. [[CrossRef](#)]